International Journal of Mechanical, Industrial and Aerospace Sciences
ISSN: 2517-9950
Vol:14, No:11, 2020

Finite Element Modelling of a 3D Woven Composite for Automotive Applications

Ahmad R. Zamani, Luigi Sanguigno, Angelo R. Maligno

***Abstract*—**A 3D woven composite, designed for automotive applications, is studied using Abaqus Finite Element (FE) software suite. Python scripts were developed to build FE models of the woven composite in Complete Abaqus Environment (CAE). They can read TexGen or WiseTex files and automatically generate consistent meshes of the fabric and the matrix. A user menu is provided to help define parameters for the FE models, such as type and size of the elements in fabric and matrix as well as the type of matrix-fabric interaction. Node-to-node constraints were imposed to guarantee periodicity of the deformed shapes at the boundaries of the representative volume element of the composite. Tensile loads in three axes and biaxial loads in *x-y* directions have been applied at different Fibre Volume Fractions (FVFs). A simple damage model was implemented via an Abaqus user material (UMAT) subroutine. Existing tools for homogenization were also used, including voxel mesh generation from TexGen as well as Abaqus Micromechanics plugin. Linear relations between homogenised elastic properties and the FVFs are given. The FE models of composite exhibited balanced behaviour with respect to warp and weft directions in terms of both stiffness and strength.

***Keywords*—**3D woven composite, meso-scale finite element modelling, homogenisation of elastic material properties, Abaqus Python scripting.

I. Introduction

AUTOMOTIVE industry has benefitted from advantages of the composite materials. They offer reduction of cost and weight while improving performance in terms of stiffness and strength of the parts among other advantages . Woven composites are widely used in auto-sector, while 3D Woven Composites (3WCs) are poised to add a new dimension to the applicability of the composite materials. Composites with 3D woven reinforcements have the potential to yield higher FVF, better out of plane stiffness and strength as well as avoidance of (interlaminar) delamination [1]-[5]. Thus, research into understanding the mechanical behaviour of 3DWCs can be important for advancement of composite technology and broadening of their range of applications. Woven fabrics are used alongside braided, knitted and non-woven reinforcements . There are many definitions for a 3D fabric . One such definition is given by . An early review of applications for 3D is given by . Overall view of the numerical approaches for analysis of 3D composites can be found in , and also .

3D fabrics can be woven is vast variations. This makes the geometry of the composites challenging for mathematical or computational modelling. Here, a 3D layer-to-layer fabric is analysed by FE method using Abaqus FE solver in the context of CAE. The fabric weave, as illustrated in Fig. 1, has been designed by MWright & Sons ltd. for the purpose of automotive parts. It shows that two warp layers and three weft layers are woven together by two layers of binder yarns, which are interleaved between warp yarns with a ratio of one to one. There are four yarns in each warp and weft layer. In fact, two Representative Volume Element (RVE) of the composite are displayed in Fig. 1, along the warp axis, namely in terms of weft columns.

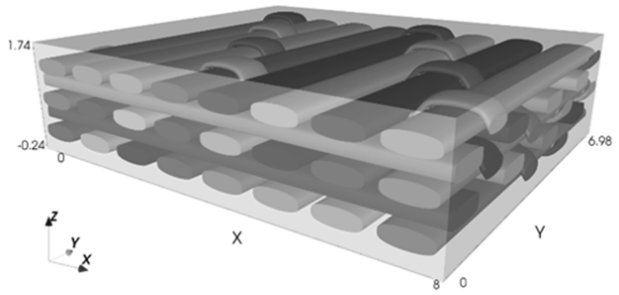

Fig. 1 Geometric model of the weave design in TexGen (dimensions in mm)

The woven fabric has been used to produce composite samples. FE analysis of these samples is presented in this article. In this study, three geometric models were built and analysed using Abaqus with five different Intra-Yarn Fibre Volume Fractions (IYFVFs). Three different methods are also applied for ensuring periodicity at the boundaries of the RVE. Definitions for volume fractions are given in Subsection II *B*, while details of the constituent materials of the composite are given in Section III.

II. Geometric Modelling

A. Adjustment of the Geometric Model in TexGen

TexGen [9], [10] and WiseTex are prominent among software for geometric modelling and visualisation of textiles, fabrics and composites. TexGen is a free and open source software and is used in this study, e.g. for rendering of the design model in Fig. 1. To evaluate the actual fabric structure, a piece of the composite was CT scanned. Fig. 2 shows a

A. R. Zamani is with the Institute for Innovation in Sustainable Engineering (IISE), University of Derby, UK (e-mail: a.zamani@derby.ac.uk).
L. Sanguigno is a research fellow at the IISE, University of Derby, UK (e-mail: l.sanguigno@derby.ac.uk).
A. R. Maligno is the Research Chair in Composite Materials at the IISE, University of Derby, UK (e-mail: a.maligno@derby.ac.uk).
This work has been conducted as part of the TMAP project, which is funded by Innovate UK (part of UK Research and Innovation).

volume rendered model of the yarns in the composite which is made using North Star Imaging visulaisation software.

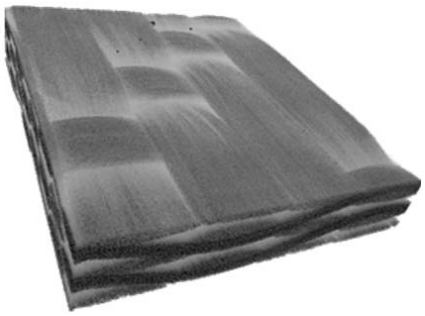

Fig. 2 Internal structure of the composite

Measurements were made on the dry fabric, composite sample as well as the CT scanned images. The geometry of the composite RVE was adjusted according to the measurements using TexGen. The model of the RVE is half of that in the design model (see Fig. 1, which shows two RVEs) in *y* (weft) direction. FE mesh of this adapted model is shown in Fig. 3, as well as Fig. 4.

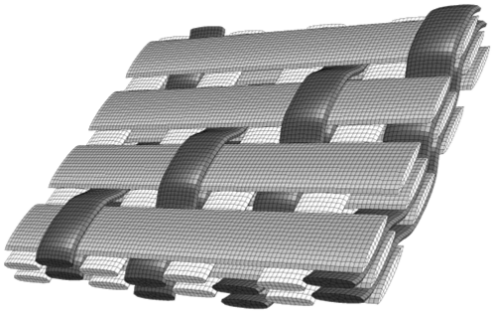

Fig. 3 Hexahedral meshing of embedded model the reinforcement

The dimensions for this RVE are: 11.0 mm × 13.0 mm × 2.16 mm along *x*, *y* and *z* directions respectively. Geometric models made in preprocessors such as TexGen and WiseTex and FE model which are directly meshed from them, are usually referred to as ideal or idealised models. Such are the models in Figs. 3 and 4. The third model in this article is a *voxel* model of the composite, exported directly from TexGen as an Abaqus input file (.inp). A corner of the RVE from this voxel model is displayed in Fig. 5 (a), while Figs. 5 (b) and (c) are showing the cross sections of the binder yarns and weft yarns respectively. In Figs. 3-5 shade of binder yarn(s) is the darkest, warp yarns' the lightest, with the weft yarn in between. Figs. 5 (b) and (c) are displayed only to emphasise the variation among those cross-sections, which are supposed to be the same. In Figs. 5 (b) and (c) boxes are put around the sections to emphasise that their relative positions outside the boxes are not preserved. The warp yarn sections are excluded; because their sections have been uniform. This variation in the cross-section is obviously reflected in the volume of the yarns: the volume of the weft yarns had two values of 5.72 mm^3 or 5.12 mm^3, i.e. over 10% difference. For binder yarns, volumes were 5. 18 mm^3 and 5.39 mm^3. All warp yarns had a volume of 5.49 mm^3. In the voxel model, the thickness of the fabric was the same as that of the RVE, i.e. no layer of resin covered top or bottom of the entire fabric.

TexGen can also write the geometric definitions to a format of machine and human readable files with the extension .tg3. They are s type of eXtensible Markup Language, XML, which are self-contained and can be used to extract the necessary information to build the geometries. Tools were made to read these files into CAE as is described in the Subsection II *A*.

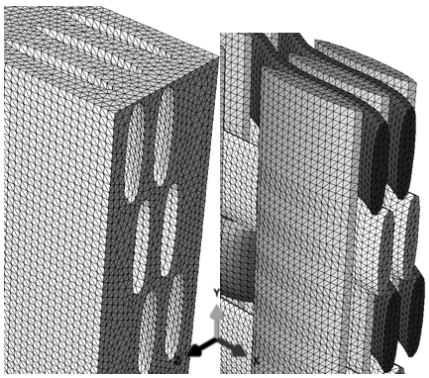

(a) (b)

Fig. 4 Tetrahedral meshing of partitioned model of the RVE: (a) matrix and (b) fabric

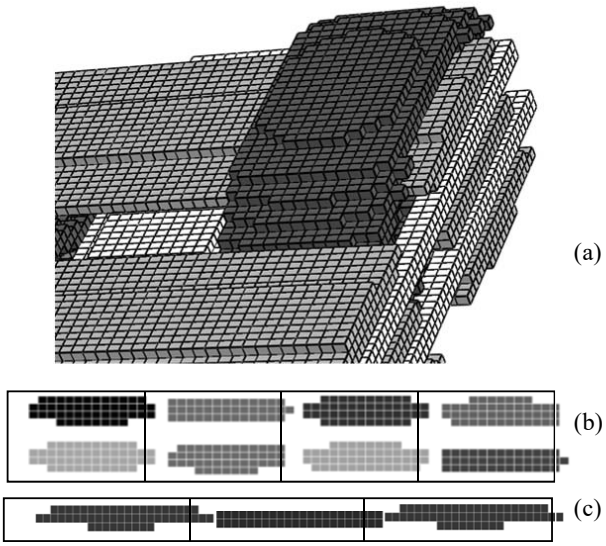

(a) (b) (c)

Fig. 5 Voxel mesh of the RVE: (a) a corner of fabric, (b) cross sections of binder yarns and (c) cross sections of a weft column

A. CAE Geometries from TexGen File

CAE has powerful geometric capabilities in its Part module as well the Assembly module. CAE also offers an Application Programming Interface (API) in Python. Python is a general-purpose and versatile programming language, which is used as API language in many other applications as well. The Python API permits the users to automate tasks like building

geometries among many others.

Here, the Python API of the CAE was used to write a module of scripts which can read a TexGen .tg3 file or a WiseTex .wfax file and build geometries in the CAE as defined in the file. A user menu is devised to allow the user define some attributes of the model such as: 1) scale factor for the yarn, 2) number of partitions per each yarn, 3) scale factor for domain, 4) element type e.g. beam or solid, 5) seed (element) size, and also 6) how yarns are modelled in the RVE. These options were used to add two layers of resin, each 0.05 mm thick, over the top and under the bottom of the fabric in the thickness (*z*) direction.

The geometry of the RVE is then built either: a) as a single part with yarns cut out of the domain as partitions, or b) with yarns as individual parts embedded in the (intact) domain. The scripts can accommodate tie or other surface-to-surface interactions between fabric and matrix, which have not been used in the presented work. For the embedded model, an *embedded region* constraint has been applied in the CAE. Fabric yarns were designated as the embedded region and the matrix as the host region. In the rest of this article case a) is referred to as *partitioned* model and case b) as *embedded*. The mesh in Fig. 3 is in fact of the fabric in embedded model, while Figs. 4 (a) and (b) show meshes of the partitioned RVE model.

Mechanical behaviour of the yarns is not isotropic, therefore, to account for its directionality, material orientations are assigned automatically for each yarn by the scripts. To do this, each yarn in divided into a user-defined number of partitions and a coordinate system is assigned to each partition with its *x*-axis along the path of the yarn. Fig. 6 shows the material orientations when assigned to a binder yarn, with arrows pointing toward the *x* direction.

Fig. 6 Material orientations on a binder yarn

The model geometry is meshed according to the user's choice. No curvature control was used in the meshing of the presented models. The sizing of the meshes is given in Table I. Given the complexity of the partitioned model, there could be only tetrahedral (or maybe wedge) elements whereas for the embedded model, hexahedral meshes were easily achieved for all yarns. TexGen is capable of exporting mesh of the dry fabric for Abaqus. However, the current scripts accommodate more choices including having mesh curvature control enabling/disabled or change of the element type and size. The mesh of the partitioned model was also used with Abaqus Micromechanics plugin for homogenization of material properties.

B. Volume Fractions for Yarn(s), Fibre and Fabric

It should be made clear that here, different types of *volume fraction* are dealt with: 1) IYFVFs, i.e. the volumetric ratio of the fibre content in a yarn, (could also be called *yarn* FVF), 2) *Yarn Volume Fraction* (YVF), which means the ratio of the volume of the yarn(s) to the total composite volume, and 3) FVF, or the ratio of the volume of fibre content in a piece of composite to the total volume. Also, *Fabric Volume Fraction* (FabVF) can be defined as the sum of all YVFs. Details of YVFs for the three models are provided in Table I. Here, IYFVF is deemed as constant for all yarns. Therefore, for the whole RVE, IYFVF times YVF give FVF. This could be used to simply convert IYFVF to FVF wherever needed in this article.

TABLE I
SEED SIZING OF THE MESHES

Model	Embedded	Partitioned	Voxel
Seed size	0.15 (all sides*)	0.12 (sides*)	0.085 × 0.098 × 0.12*

* All in mm

TABLE II
YVFS

Model	Type	Warp	Weft	Binder	Total
TexGen	Solid	0.133	0.222	0.137	0.492
CAE	Solid	0.121	0.201	0.125	0.447
Embedded	Mesh	0.116	0.196	0.119	0.431
Partitioned	Mesh	0.119	0.199	0.123	0.441
Voxel	Mesh	0.156	0.210	0.137	0.503

III. MATERIAL PROPERTIES

The fabric was woven from carbon fibre yarns of product No. T700S by Torayca®. The matrix material has been Elium® thermoplastic resin by Arkema. Here, static loading conditions have been considered and thermal properties of the Elium® are ignored. Properties of the constituents are mentioned in Table III. Yarns were of type 12K, meaning that each yarn was made of approximately twelve thousand carbon fibres. Mechanical properties of the materials are recorded in Table III, which were used in the analyses. A simple damage model based on the Maximum Principal Stress (MPS) criterion was applied to both materials using the ultimate stress (S_u) values in Table III . Element deletion option was activated which would delete the elements that have had the principal stress in their material points exceed S_u. The damage model was not applied to the voxel model and it was analysed as exported by TexGen with no modification. TexGen generates Abaqus input files with a voxel model for homogenisation of material properties and the analysis step is of *linear perturbation* type which is not to be used for damage modelling.

TABLE III
PROPERTIES OF CONSTITUENT MATERIALS OF THE COMPOSITE

Material	E_1 [GPa]	E_2=E_3 [GPa]	υ_{12}= υ_{13}	G_{12}=G_{13} [GPa]	G_{23} [GPa]	S_u [GPa]
Fibre (T700)	230.0	15.0	0.20	24.0	5.0	4.9
Resin (Elium®)	3.3	3.3	0.35	1.2	1.2	0.076

A. Microscale Simulation

Material properties of the yarns cannot be described as

fibre-only, because of their resin content. Thus, to have material properties for the yarns, microscale FE models of the hexagonal arrangement of carbon fibres were made using Abaqus Micromechanics plugin. Five IYFVFs are presented, namely 0.2, 0.4, 0.6, 0.8 and 0.88. The latter (0.88) was chosen as because it is close to the maximum value allowable in a hexagonal arrangement. Microscale FE models of two IYFVF are shown in Fig. 7. There, interphase layers between the fibre cross sections and the matrix are highlighted in brighter shade of grey as rings around the fibre. Nonetheless, the presence of this interphase is merely geometric, and the material properties of the interphase were chosen the same as the matrix.

Results from microscale computations as given in Table IV, were used as material properties for mesoscale FE computations to evaluate parameters, such as elastic moduli and strength of the RVE for different FVFs. The models were analysed for to get homogenized properties to be used as material properties for the yarns.

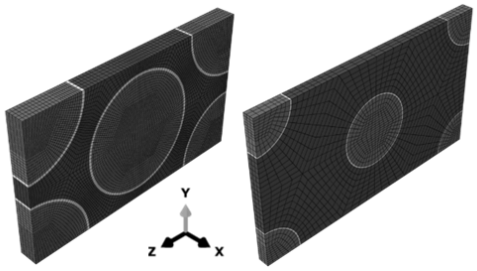

(a) (b)

Fig. 7 Microscale models for two IYFVFs: (a) 0.2 and (b) 0.6

TABLE IV
MATERIAL PROPERTIES FOR THE YARNS

IYFVF	E_1 [GPa]	E_2=E_3 [GPa]	υ_{12}= υ_{13}	G_{12}=G_{13} [GPa]	G_{23} [GPa]	S_u [GPa]
0.2	48.6	4.6	0.32	1.8	1.5	1.0
0.4	94.0	5.8	0.28	2.6	1.9	2.0
0.6	139.3	7.7	0.25	4.1	2.6	3.0
0.8	184.7	10.5	0.23	8.0	3.5	3.9
0.88	202.8	12.1	0.21	12.7	4.1	4.3

IV. BOUNDARY CONDITIONS

Different approaches can be taken to ensure the periodicity at the boundaries of an RVE. Here, when using Abaqus Micromechanics plugin (which is used for the model named partitioned/plugin model in the tables) and TexGen voxel model, their own default methods were applied as intended. For embedded and partitioned models, the approach was as follows:

The RVE is assumed to be a right-angled hexahedron (cuboid) and that it has L_x, L_y and L_z as its dimensions along the x, y and z axes. Periodicity at the RVE boundaries, i.e. its bounding surfaces normal to x and y, and z axes, can be guaranteed by imposition of equation constraints on each pair of corresponding nodes on opposing faces of the RVE . Equation constraints were applied to the opposing nodes, so that:

$$\begin{aligned} u_1(0,y,z) - u_1(L_x,y,z) &= L_x\varepsilon_x \\ u_2(x,0,z) - u_2(x,L_y,z) &= L_y\varepsilon_y \\ u_3(x,y,0) - u_3(x,y,L_z) &= L_z\varepsilon_z \end{aligned} \quad (1)$$

In (1), u_x, u_y, u_z stand for displacements, and ε_x, ε_y, ε_z for strains in x, y and z directions. Three reference nodes were created, which control the strains (and therefore the displacements) along the three axes. Hence, axial loading conditions in each direction can be applied only to the corresponding reference point with its magnitude equal to the desired strain. This approach can be deemed as a more rigorous one, since it applied constraints to almost all nodes on the RVE boundaries, compared to those adopted by Micromechanics plugin or TexGen.

V. RESULTS

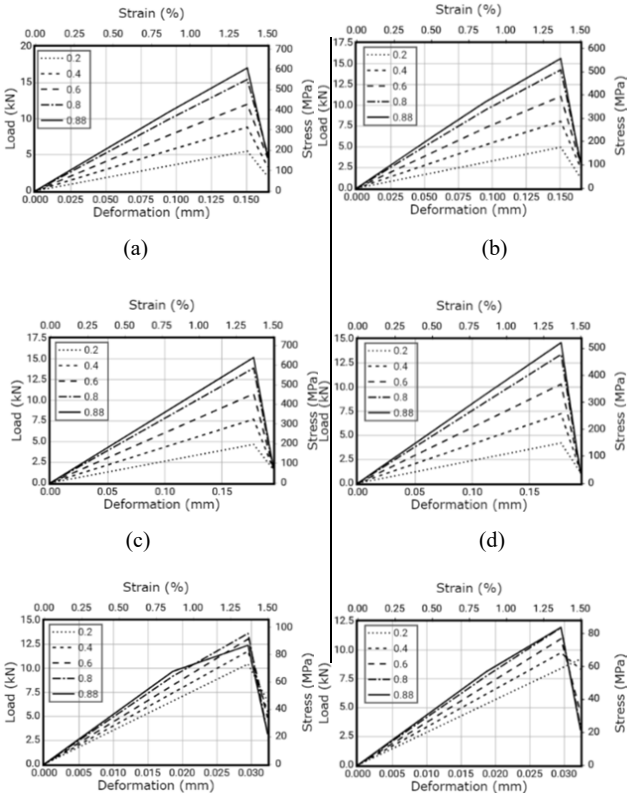

Fig. 8 Load-displacement and stress-strain plots: (a) embedded, load in x-direction, (b) partitioned, x-direction, (c) embedded, y-direction, (d) partitioned, y-direction, (e) embedded, z-direction, and (f) partitioned, z-direction

Results for load-deformation and stress-strain from different analyses are plotted in Fig. 8. Deformed shape of loading of an RVE in the weft or y-direction from partitioned model is displayed in Fig. 9. It shows damage in the matrix (prior to any damage in the fabric) as deleted elements. The streak of these deleted elements is seen to be aligned with the path of

the binder yarns. Young's moduli in each direction are also extracted and tabulated in Table V, whereas values for ultimate strength are listed in Table VI.

A linear curve fitting was applied to the results in Table V, and the lines plotted in Fig. 10. The parameters defining these lines are provided in Table VII.

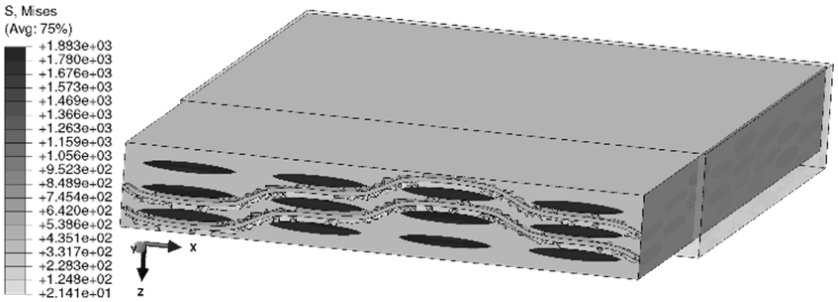

Fig. 9 Deformed/undeformed shapes of the RVE of the partitioned model in tensile loading in *y* direction, with stress levels (in MPa) plotted on the deformed shape (deformation scale: ×50)

A refinement of the mesh of the embedded model from 0.15 mm to 0.10 mm, as well as a courser mesh with seed size of 0.2 mm was tried. A refined mesh with seed size of 0.10 mm was also tried for the partitioned model. No significant changes in the results were observed due to these changes in mesh sizing.

TABLE V
ELASTICITY MODULI (E_1, E_2, E_3)

MODEL	YVF				
	0.20	0.40	0.60	0.80	0.88
			E_1		
Embedded	14.3	23.2	31.9	41.0	45.2
Embedded/biaxial	16.3	25.0	33.6	42.9	47.1
Partitioned	12.9	21.5	30.1	39.3	43.4
Partitioned/biaxial	14.2	22.8	31.4	40.7	44.9
Partitioned/plugin	12.5	20.4	28.3	36.5	40.1
Voxel	13.6	22.8	31.7	41.2	45.4
			E_2		
Embedded	14.3	23.7	33.1	43.0	46.7
Embedded/biaxial	16.3	25.5	34.9	44.7	48.7
Partitioned	12.9	22.2	31.7	41.3	45.3
Partitioned/biaxial	14.2	23.5	33.0	42.8	46.7
Partitioned/plugin	12.9	22.2	31.7	41.3	45.2
Voxel	13.3	23.3	33.3	43.5	47.7
			E_3		
Embedded	5.3	6.0	6.7	7.4	7.4
Partitioned	4.3	5.0	5.6	6.3	6.6
Partitioned/plugin	4.6	5.4	6.1	6.8	7.1
Voxel	4.7	5.6	6.4	7.2	7.5

VI. DISCUSSIONS

A. Geometric Models

Embedded element approach is a way to simplify the task of geometric modelling. No issue related to this simplification is observed in the results, compared to the more geometrically precise model with the partitioned geometry. The embedded region technique seems to have been robustly implemented by Abaqus. It has been reported to have been successfully applied in composite simulations by [14]-[16]. However, Abaqus Micromechanics plugin does not seem to support embedded regions technique with ease. Here, an implementation of periodicity for the RVE boundaries based on the free and open source tool HomTools , is used which has worked with no issues. The script of modules developed for generating mesh of the meshes for the RVE supports shell and wire/beam elements as well solid elements for the reinforcement fabric.

The partitioned model (see Fig. 4) is the most geometrically detailed and accurate one. It affords a clear-cut and distinct geometry for the matrix, which make it more suitable for focusing on the matrix and fabric-matrix interface. The developed module allows the fabric-matrix interface to be defined in ways other than partitioning, e.g. by imposition of tie constrain between them or other contact definitions. The option to change the mesh using curvature control is also available, while the hexahedral elements mostly are unavailable.

For the voxel model, the cross-section of the binder and weft yarns have varied as described subsection above and illustrated in Figs. 5 (b) and (c). The effect of this variation especially in other loading conditions needs further investigation.

TABLE VI
ULTIMATE STRENGTH

MODEL	YVF				
	0.20	0.40	0.60	0.80	0.88
			Su_1 (*x*-direction)		
Embedded	196	314	428	551	608
Embedded/biaxial	167	256	342	434	478
Partitioned	176	287	395	509	558
Partitioned/biaxial	146	233	314	401	441
			Su_2 (*y*-direction)		
Embedded	196	324	454	585	640
Embedded/biaxial	167	262	358	457	498
Partitioned	176	305	434	564	616
Partitioned/biaxial	146	241	338	435	474
			Su_3 (*z*-direction)		
Embedded	73	82	91	96	86
Partitioned	64	68	77	84	84

Results in Fig. 10 reveal that embedded model consistently

has yielded higher values for moduli, followed by the voxel model, with the partitioned model giving the lowest values. Table VI shows that between the two models analysed for strength, embedded model again has given higher vales than the partitioned model.

B. Biaxial vs Uniaxial Loading

Biaxial loading has been shown to have been able to raise the moduli in both directions by up to 15% compared to the corresponding uniaxial loading while the ultimate strength from the uniaxial loadings has been shown to be up to 20% higher as compared to those from biaxial loading. The lowering of ultimate strength is expected and is simply owed to combined stresses in biaxial loading.

TABLE VII
PARAMETERS FOR LINES FITTED TO MODULI AGAINST IYFVF

	E_1	E_2	E_3
Embedded	(5.1, 45.1)	(4.6, 47.8)	(4.7, 3.2)
Partitioned	(3.7, 44.6)	(3.2, 47.6)	(3.6, 3.3)
Voxel	(4.2, 46.5)	(3.1, 50.5)	(3.9, 4.1)

Given (a_0, a_1) pairs define lines as: $y = a_0 + a_1 x$

C. Effect of FabVF

Results in Tables V and VII and Fig. 10 show that for *x* and *y* directions, the difference among results for elastic moduli from the three geometric models are not large relative to their magnitudes. Nonetheless, for the z direction, the relative difference among the results is more noticeable. Pair of coefficients in Table VII can be used to estimate stiffness moduli for a given volume fraction, e.g. by extrapolation.

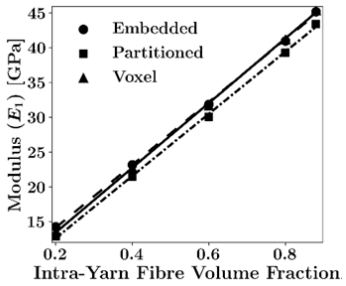

(a)

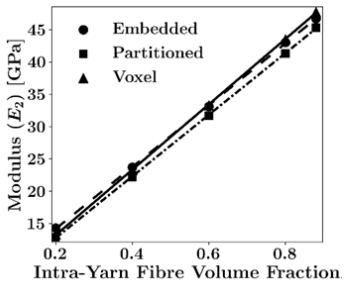

(b)

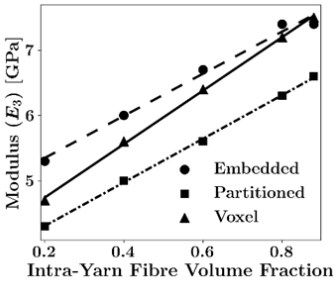

(c)

Fig. 10 Lines fitted to the Young's moduli-IYFVF results in Table V: (a) E_1, (b) E_2 and (c) E_3

D. Damage and Failure

The applied damage model was based on the MPS criterion, i.e. elements were deleted when the MPS in them exceeds the given values in Table III for matrix and Table IV for yarns. Plots in Fig. 8 show almost a linear behaviour until sudden failure (except for the loading in z-direction at IYFVF of 0.88). This means that the failure of the matrix, which has occurred at a much lower stress level than the ultimate strength, has not been easily detectable in the stress-strain curves in Fig. 8. This is plainly a result of the yarns not only providing overwhelmingly the strength of the composite, but also doing the same vis-à-vis stiffness. Strength and stiffness values for matrix in Table III compared to those of the yarns in Table IV would reveal that even for the lowest IYFVF of 0.2, yarns happen to be both the stronger and the stiffer component by a factor of ten. Size of increments in the steps of all analyses was set automatically by the Abaqus Standard solver. As a result, the number of the increments was 5 to 7. A higher number of increments could change the results for strength values by up to 15%.

As seen in Fig. 9, damage in the matrix starts at much lower load level (especially for higher values of IYFVF), mostly around the binder yarn. So, binder yarns are confirmed as a source of weakness, which has been pointed out previously e.g. by .

E. Warp v Weft Directions

Comparing plots in Figs. 10 (a) to (b) will show a balanced stiffness behaviour in terms of warp versus weft directions. Results in Table V show that at higher IYFVFs, E_2 values were only slightly higher than E_1 values. This is supported by values in Table VII, which show that coefficients for E_2 (multiplicands of IYFVF, i.e. second item of the pairs) are 5 to 10% higher for E_2 relative to E_1.

Plots in Fig. 8 and results in Table IV show the same balanced behaviour in terms of ultimate strength with the strength in the weft direction surpassing that of the warp direction, by 5 to 10% for higher IYFVFs.

VII. CONCLUSION

A 3D composite which has been designed to be used for parts in automotive industry is analysed by FE method using

Abaqus software package. New tools for generating solid 3D FE meshes of the fabric/matrix are presented. They can read TexGen and WiseTex files and build FE models of the fabric/ matrix in Abaqus/CAE. User-menu is offered to define the FE model in terms of type of the model, interactions, elements and material orientations. Three geometric models, five fibre/ FabVF as well three methods for ensuring periodicity at the RVE boundaries were used.

Results for homogenised elastic moduli and ultimate strengths are presented. Differences and similarities among these models and methods are highlighted. Embedded element technique, as implemented by Abaqus, found to provide a straightforward approach, with good quality for the meshes. Although in terms of computational expense, it is not optimum, due to matrix elements which coincide with the fabric elements. Partitioned model offers a geometrically more accurate FE mesh. Also, for matrix-fabric interactions, the partitioned model provides more choices and accuracy because there is room for clear surface-to-surface interaction definitions and options like tie constraint and contact definitions being afforded.

In terms of periodicity on RVE boundaries, node-to-node constraints were easily applicable (using a script) where Abaqus plugin could not be used with ease (e.g. with embedded elements).

Linear relations between fibre/FabVF and elasticity moduli were highlighted, which can estimate the moduli. For volume fractions above the values afforded by the idealised models, extrapolation can give a working approximation.

Results demonstrated a balanced behaviour in terms of stiffness and strength in warp and weft directions, with weft direction getting slightly stiffer and stronger at higher volume fractions.

This study shows the extent of applicability of FE models based on idealised geometric models by software such as TexGen for a 3D composite with layer-to-layer woven reinforcement.

Acknowledgment

The composite fabric has been designed and manufactured by MWright and Sons ltd. (https://www.mwright.co.uk). Composite samples were produced by both MWright & Sons and Far-UK ltd (https://www.far-uk.com). Surface treatment of the fabric was conducted by Oxford Advanced Surfaces (https://www.oxfordsurfaces.com). This work has been part of the TMAP project, which is funded by the Innovate UK.

References

[1] M. Ansar, W. Xinwei and Z. Chouwei, "Modeling strategies of 3D woven composites: A review," Compositer Structures, vol. 93, no. 8, pp. 1947-1963, July 2011.
[2] X. Chen, L. Waterton and L.-J. Tsai, "An overview of fabrication of three-dimesional woven textile preforms for composites," Textile Research Journal, vol. 81, no. 9, 2011.
[3] N. S. Karaduman, Y. Karaduman, H. Ozdemir and G. Ozdemir, "Textile Reinforced Structural Composites for Advanced Applications," in Textiles for Advanced Applications, InTech, 2017, pp. 87-133.
[4] H. M. El-Dessouky and N. Saleh, "3D Woven Composites: From Weaving to Manufacturing," in Recent Developments in the Field of Carbon Fibers, 2017, pp. 51-66.
[5] L. Ciobanu, "Development of 3D Knitted Fabrics for Advanced Composite Materials," in Advances in Composite Materials - Ecodesign and Analysis, 2011.
[6] P. Ünal, "3D Woven Fabrics," 2012, pp. 91-120.
[7] A. P. Mouritz, M. K. Bannister, P. J. Falzon and K. H. Leong, "Review of applications for advanced three-dimensional fibre textile composites," Composites: Part A, vol. 30, p. 1445–1461, 1999.
[8] T. Gereke and C. Cherif, "A review of numerical models for 3D woven composite reinforcements," Composite Structures, vol. 209, pp. 60-66, 1 February 2019.
[9] X. Zeng, L. P. Brown, A. Endruweit, M. Matveev and A. C. Long, "Geometrical modelling of 3D woven reinforcements for polymer composites: Prediction of fabric permeability and composite mechanical properties," Composites: Part A, vol. 56, pp. 150-160, 2014.
[10] M. Sherburn, "Geometric and Mechanical Modelling of Textiles," 2007.
[11] S. V. Lomov, "WiseTex software suit," 2013.
[12] S. Dhiman, P. Polturi and C. Silva, "Influence of binder configuration on 3D woven composites," Composite Structures, vol. 134, pp. 862-868, 2015.
[13] S. Lejeunes and S. Bourgeois, "Une Toolbox Abaqus pour le calcul de propriétés effectives de milieux hétérogènes," in 10e colloque national en calcul des structures, Giens, France, 2011.
[14] S. A. Tabatabaei and S. V. Lomov, "Eliminating the volume redundancy of embedded elements and yarn interpenetrations in meso-finite element modelling of textile composites," Composite Structures, vol. 152, pp. 142-154, 2015.
[15] S. A. Tabatabaei, S. V. Lomov and I. Verpoest, "Assessment of embedded element technique in meso-FE modelling of fibre reinforced composites," Composite Structures, vol. 107, pp. 436-446, January 2014.
[16] A. Y. Matveeva, H. J. Böhm , G. Kravchenko and F. W. J. van Hattum, "Investigation of the Embedded Element Technique for Modelling Wavy CNT Composites," vol. 42, 2014.